

## SCALING OF TURBULENT BOUNDARY LAYER PROFILES IN AIRFLOW OVER YOUNG WIND-WAVES

**Meital Geva**

School of Mechanical Engineering  
Tel-Aviv University  
Tel-Aviv 69978, Israel  
meitalgeva@mail.tau.ac.il

**Lev Shemer**

School of Mechanical Engineering  
Tel-Aviv University  
Tel-Aviv 69978, Israel  
shemerl@tauex.tau.ac.il

### ABSTRACT

Understanding the air velocity profile over wind-waves is crucial for evaluation of momentum and energy transfer between air and water. It is well accepted that the airflow above water waves has logarithmic profile that is usually expressed in terms of an effective roughness parameter. This parameter however cannot be evaluated directly from the wave measurements at the water surface. Determination of accurate air velocity profile in field conditions is nearly impossible; the existing estimates are based on rough data. We suggest an alternative approach based on the extensive experimental data accumulated in our wind-wave facility. Combined measurements of the finely resolved mean air velocity profile above water surface and of the characteristics of the wind-wave field were performed at 6 wind forcing conditions and at 7 fetches. We demonstrate that the spatially developing boundary layer over the complicated three-dimensional, random and moving wind-wave surface is characterized by wall similarity observed in turbulent flow above rough solid surfaces. The results enable more accurate estimations of the actual drag coefficient.

### INTRODUCTION

The coupling between air and water in the presence of wind-waves determines mass and momentum transfer between atmosphere and ocean and thus controls the weather and, to a large extent, determines the life conditions, in particular in oceans. In wind waves studies, the generally accepted air velocity profile is:

$$U(z) = \frac{u_*}{\kappa} \ln \left( \frac{z}{z_0} \right) \quad (1)$$

where  $u_*$  is the friction velocity determined by the shear stress at the water surface,  $\tau_w$ , and the air density  $\rho$ ,  $u_* = \sqrt{\tau_w/\rho}$ . The friction parameter  $z_0$  is a function of the roughness density. Both  $u_*$  and  $z_0$  are obtained from experiments; however, the available field and laboratory data lack sufficient resolution, e.g., Hristov *et al.* (2003); Caulliez *et al.* (2008)

and references therein. Moreover,  $z_0$  cannot be directly evaluated from the water surface features (Csanady, 2001), it is often estimated using the Charnock relation,  $\alpha_{ch} = z_0 g / u_*^2$  (Charnock, 1955). Here  $\alpha_{ch}$  is presumably constant and  $g$  is the gravitational acceleration. It was found however that  $\alpha_{ch}$  is in fact not constant and may vary by two orders of magnitude (Bye *et al.*, 2010). Although there were numerous ongoing attempts to relate  $z_0$  to wind-waves characteristic, no universal formulation was found so far. The wind-wave field varies continuously in time and space; thus the water surface has time-dependent random three-dimensional topography (Zavadsky & Shemer, 2017). Although water waves statistics can be obtained relatively easily, measurements of the air flow over a moving stochastic three-dimensional wavy surface are more challenging (Zavadsky & Shemer, 2012). While the data on air flow over wind-waves is limited, more extensive information is available on flow over rough solid surface with diverse topographies, see Chung *et al.* (2021) for a recent review. These studies indicate that when the roughness effects are limited to the near wall region, the boundary layers in free and bounded flows experience similarity, e.g., Shockling *et al.* (2006); Schultz & Flack (2007) and references therein. Jimenez (2004) asserted that similarity may be found when the ratio between the roughness height and boundary layer thickness is above 40, whereas Castro (2007) observed that wall similarity holds up to a limit of 5. Flack & Schultz (2014) showed that this limit depends on the shape of the roughness elements. Albeit fundamental differences between the solid rough surface and the wavy water surface exist, we found essential common features characterizing the turbulent boundary layers in these cases, providing an alternative insight on the air-water coupling.

### WIND-WAVE EXPERIMENTS

#### The facility

Experiments were conducted at the Tel-Aviv University wind-wave facility described schematically in Figure 1. The facility consists of a closed-loop wind tunnel atop of a 5 m long rectangular test section. The test section is 0.4 m wide

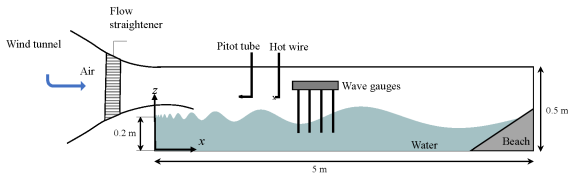


Figure 1. Schematic illustration of the TAU wind-wave facility.

and 0.5 m high; it is filled with water to depth of 0.2 m. The airflow uniformly enters the test section after passing through a large settling chamber, honeycomb and converging nozzle with an area reduction ratio of about 4. The instantaneous surface elevation  $\eta(x,t)$  is recorded at several downstream locations using capacitance-type wave gauges that are positioned at the centreline of the test section. The mean airflow is measured using a pitot tube with an outer diameter of 1 mm. The vertical profiles of the turbulent fluctuations are obtained using an X-hot film. The pitot tube and the hot-film are supported by a vertical computer-controlled stage that allow precise positioning. To keep both sensors dry, measurements above the water surface were restricted to elevations above the maximum possible wave crest. The accuracy of the probe positioning is 0.05 mm; measurements were performed at up to nearly 100 vertical locations  $z$ . The data acquisition lasted from few minutes for wind velocity measurements at each  $z$ , to an hour or more for surface elevation  $\eta(x,t)$ . The acquisition duration was thus larger by orders of magnitude than the characteristic wind-wave periods that range from 0.1 s to 1.5 s. The experiments were performed at 6 wind forcing conditions. For each maximum wind velocity  $U_0$ , the data were gathered at 7 downstream distances ranging from 1 m to 3.4 m. For more details on the experimental facility and the inherent difficulties in this kind of measurements see Liberzon & Shemer (2011) and Zavadsky & Shemer (2012).

### Characteristics of young wind-waves

Under steady wind forcing, the wave height,  $h$ , and the wavelength,  $\lambda$ , grow with the downstream distance,  $x$ , as shown schematically in Figure 2(a). Boundary layer with thickness  $\delta(x)$  is formed and develops with  $x$ . Snapshots of the air-water interface at different downstream distances presented in Figure 2(b) demonstrate the changing topography of the water-surface. Wind-waves are stochastic and three dimensional, losing their coherence fast in time as well as in space (Kumar *et al.*, 2022). The characteristic wave amplitude is defined as the rms value of the local instantaneous surface elevation  $\eta(x,t)$ . Due to wave breaking, the steepness  $\eta_{rms}k_p$  at all wind forcing conditions is limited to about  $0.2 \div 0.25$ , where  $k_p$  is the peak wave number (Zavadsky & Shemer, 2012; Hsu *et al.*, 1982; Buckley *et al.*, 2020). The average friction velocities determined for each wind forcing by two independent methods, from the velocity profiles and by measuring vertical distribution of Reynolds stresses (Zavadsky & Shemer, 2012), are presented in Table 1. Both methods to determine the friction velocity rely on a proper fitting that should be limited to the logarithmic layer ( $z/\delta < 0.2$ ). For the extreme wind conditions, Zavadsky & Shemer (2012) were forced to extend the fitting domain to  $z/\delta < 0.3$ . They acknowledge that insertion of some portion of the wake in the fit results in an unavoidable overestimate of the friction velocity. Their estimations of the friction velocities  $u_*$  are listed in Table 1 and agree well with Plant & Wright (1977) and Buckley *et al.* (2020). It was ob-

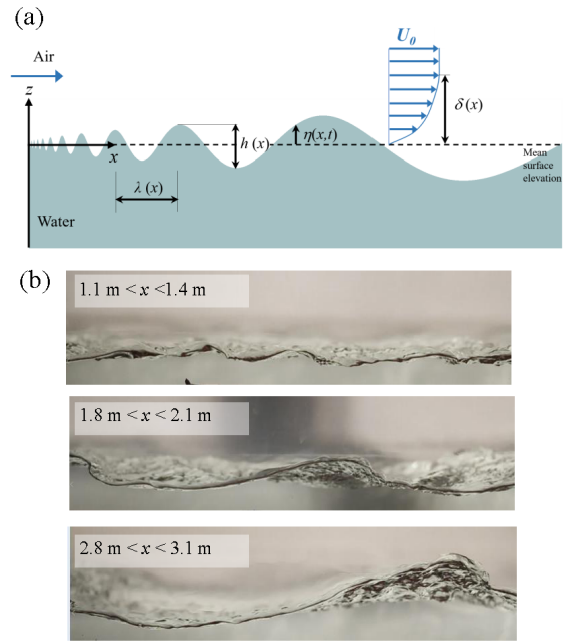


Figure 2. (a) Schematic illustration of wind-waves growth and the developing boundary-layer in air; (b) snapshots of the wave field taken through the side window of the test section at three locations at maximum wind velocity  $U_0=11.2$  m/s.

served in Zavadsky & Shemer (2012) that the variation of  $u_*$  with fetch did not exceed about 7%. The non-trivial experimental observation that  $u_*$  remains constant along the test section was also reported elsewhere (Plant & Wright, 1977; Hsu *et al.*, 1982; Caulliez *et al.*, 2008). Note that the water drift velocity is less than  $0.5u_*$  (Caulliez *et al.*, 2008; Zavadsky & Shemer, 2017).

Table 1. Characteristic mean wind velocities:  $U_0$ - the maximum wind velocity and  $u_*$  - the friction velocity. Subscript ZS represents the data from Zavadsky & Shemer (2012) and subscripts MI is the momentum integral estimations.

$U_0$ (m/s)	$u_{*,ZS}$ (m/s)	$u_{*,MI}$ (m/s)
5.5	$0.29 \pm 0.010$	$0.30 \pm 0.009$
6.6	$0.37 \pm 0.013$	$0.39 \pm 0.011$
7.7	$0.45 \pm 0.016$	$0.47 \pm 0.012$
8.9	$0.56 \pm 0.019$	$0.54 \pm 0.013$
10.05	$0.68 \pm 0.024$	$0.61 \pm 0.011$
11.2	$0.85 \pm 0.03$	$0.77 \pm 0.014$

## RESULTS

### Integral boundary layer parameters

The measured velocity profiles at seven downstream locations in the range  $1 \text{ m} \leq x \leq 3.4 \text{ m}$  for the wind forcing

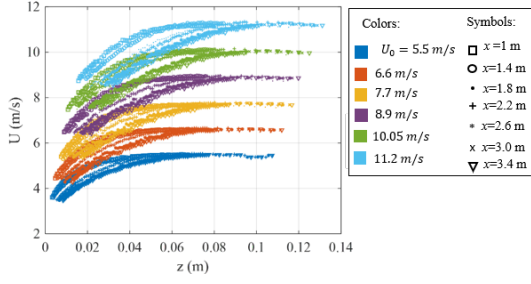


Figure 3. Mean vertical velocity profiles in air.

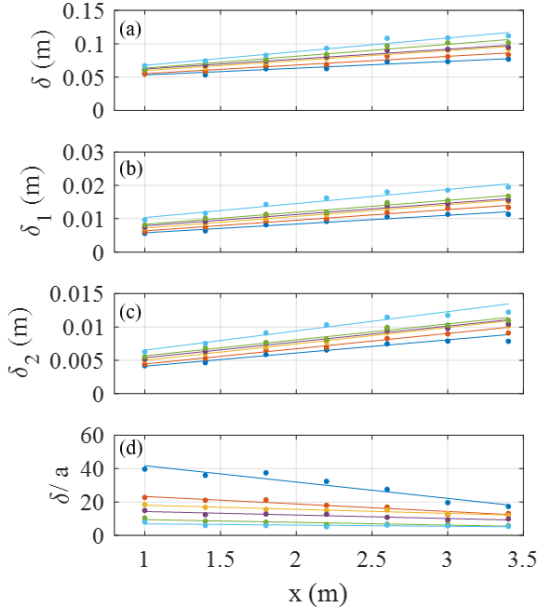


Figure 4. Boundary layer characteristics: (a) boundary layer thickness  $\delta$ , (b) displacement thickness  $\delta_1$ , (c) momentum thickness  $\delta_2$  and (d) normalized roughness height defined as  $a/\delta = \sqrt{2}\eta_{rms}/\delta$ . Colours correspond to those in Figure 3.

specified in Table 1 are plotted in Figure 3(a). It should be stressed that due to the movement and randomness of the water surface, there is an inherent difficulty to measure the wind velocity profiles adjacent to the water surface. This difficulty is more severe at the two strongest wind forcings as the wave heights increase; to keep the air velocity sensors dry, no measurements were carried out in the close vicinity of the interface at  $U_0=10.05$  m/s and 11.2 m/s.

The boundary layer thickness  $\delta$  was defined as elevation from the interface where the wind velocity reached  $0.99U_0$ . Estimation of the integral values, the displacement thickness  $\delta_1$  and momentum thickness  $\delta_2$ , require extrapolating the lower part of each velocity profile to the water surface. The fitting at elevations smaller than the available experimental data was based on the linear-logarithmic profile suggested by Miles (1957), which consists of a linear segment in the viscous sub-layer followed by a logarithmic part. The boundary layer characteristics are shown in Figure 4(a)-(c) and will be used in sequence.

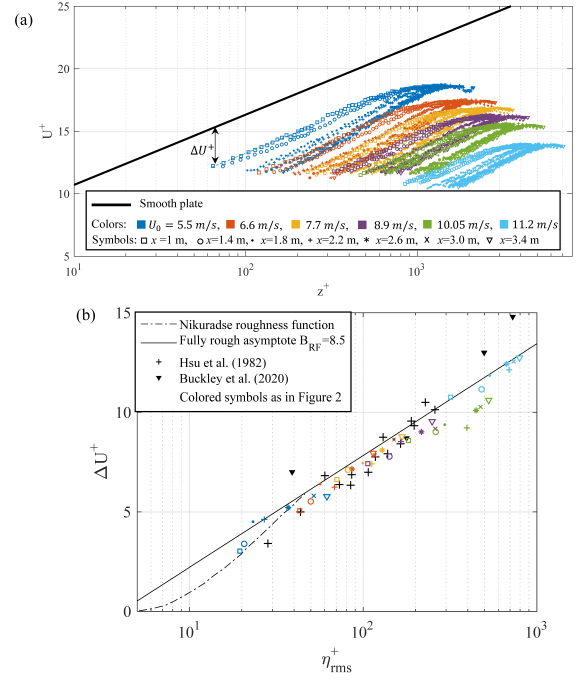


Figure 5. (a) Dimensionless mean velocity profiles at various wind velocities and fetches; (b) the downshift  $\Delta U^+$  as a function of the characteristic surface elevation.

### Boundary layer similarity

The dimensionless profiles  $U^+ = U/u_*$  as a function of  $z^+ = zu_*/\nu$  are presented in Figure 5(a) together with the velocity profile over smooth water surface represented by a bold line. Although the vertical coordinate of the measurement at the two extreme wind velocities exceeds  $z^+=300$ , it is apparent that the slopes of  $U^+(z^+)$  in the logarithmic part of the profiles in all cases are close to that over a smooth surface. It is also evident that the profiles over the wavy water surface are shifted downward relative to the bold line. The shift  $\Delta U^+$  increases with wind velocity and downstream distance. The increase in  $U_0$  and in  $x$  results in wave amplification that increases the surface's roughness. In turbulent flows over rough solid surfaces, the amount of the downshift from the smooth velocity profiles,  $\Delta U^+$ , depends on the dimensionless characteristic sand grain roughness height  $k_s^+$ . Hudson et al. (1996) analyzed the boundary layer over a deterministic solid wavy surface and used the surface amplitude as  $k_s$ . For a moving stochastic air-water interface, we select the representative wave amplitude  $\eta_{rms}(x)$  as the characteristic roughness,  $k_s(x)$ . Figure 5(b) demonstrates the values of  $\eta_{rms}(x)$  vs. the values of  $\Delta U^+$  from figure 5(a); data obtained in other facilities are added. The contribution of the surface drift velocity cancels out since  $\Delta U^+$  represents the difference in velocities over the smooth and wavy water surfaces. Nearly all markers in Figure 5(b) follow the fully rough asymptote. It is thus evident that the shapes of the mean velocity profiles in the overlap region are unaffected by the roughness  $\eta_{rms}$  which determines only their vertical shift. The velocity profile may be therefore approximated by

$$U^+(x, z) = \frac{1}{\kappa} \ln \left( \frac{z}{\eta_{rms}(x)} \right) + 8.5 \quad (2)$$

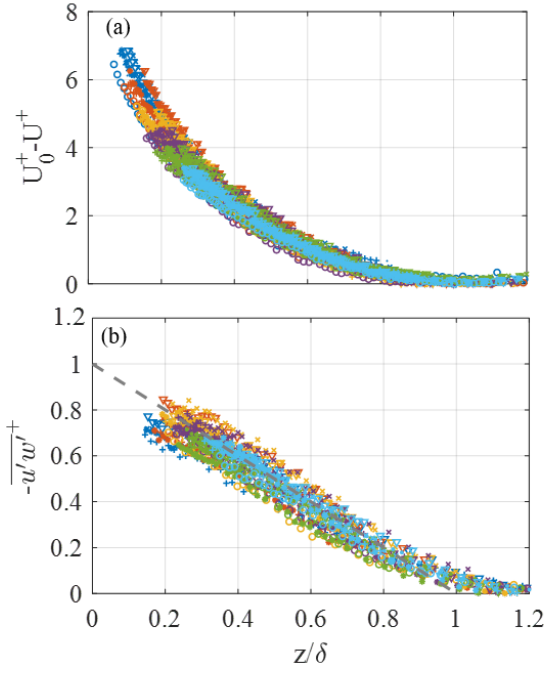


Figure 6. Evidence of wall similarity in (a) the velocity defect law and (b) normalized Reynolds stresses. Colors and markers as in Figure 3.

that unlike equation (1) contains only directly measurable quantities. The fact that the overlap and outer layers of the boundary layers are not affected by the surface roughness may also be evident in the collapse of the velocity defect profiles and the similarity in the distribution of the normalized Reynolds shear stress  $-\overline{u'w'^+}$  (Figure 6). Since the air in a rectangular tank is subjected to a favorable pressure gradient, outer-layer similarity may not be always expected. The appropriate values of Clauser parameter  $\beta$  and of the defect shape factor  $G$  are evaluated:

$$\beta = \frac{\delta_1}{\tau} \frac{dp}{dx} \quad (3)$$

$$G = \frac{u_*}{\delta_1 U_0} \int_0^\delta \left( \frac{U_0 - U(z)}{u_*} \right)^2 dz \quad (4)$$

The pressure drop  $dp/dx$  was measured directly in Liberzon & Shemer (2011) for the airflow conditions listed in Table 1; it agrees with the approximation based on Navier-Stokes relation as  $\beta = -\frac{\delta_1}{\delta} \frac{\partial(\overline{u'w'^+})}{\partial(z/\delta)} \approx -\frac{\delta_1}{\delta}$ . The values of  $\beta$  and  $G$  do not vary significantly for all operational conditions,  $\beta = -0.1 \div -0.17$  and  $G = 5.13 \pm 0.33$ . This provides further support for the wall similarity. Note that for all cases, the ratio between the roughness height, defined as  $a = \sqrt{2}\eta_{rms}$  and the boundary layer thickness is above 5 (see figure 4d) consistent with the critical value required for wall similarity (Castro, 2007).

### Skin friction estimation and the coupling between air and young wind-waves

The vertical downshift  $\Delta U^+$  represents deficit due to momentum exchange between air and water. The similarity of the

boundary layers implies that the deficit depends only on the roughness height. We utilize the momentum integral relation in the presence of pressure gradient:

$$\frac{u_*^2}{U_0^2} = \frac{d\delta_2}{dx} - (2\delta_2 + \delta_1) \frac{1}{\rho U_0^2} \frac{dp}{dx} \quad (5)$$

that can be approximated as

$$\frac{u_*^2}{U_0^2} \approx \frac{d\delta_2}{dx} + \frac{(2\delta_2 + \delta_1)}{\delta} \frac{u_*^2}{U_0^2} \quad (6)$$

For a given wind velocity  $U_0$ , substituting the values of  $\delta$ ,  $\delta_1$  and  $\delta_2$  (Figure 4a-c) into equation (6) enables additional independent estimation of the friction velocity  $u_*$  at any  $x$ . These values are listed in the right column in Table 1 and are consistent with estimates by Zavadsky & Shemer (2012). Evaluation of the friction velocities via the integral relations is more robust and less sensitive to the profile details in the lower part of the boundary layer. The friction velocities determined by this method remain nearly constant along the test section.

Equation (6) can be further used to relate the skin friction at any surface elevation. The integral values of displacement and momentum thickness,  $\delta_1$  and  $\delta_2$  respectively, can be explicitly evaluated using the vertical velocity profile. We have shown the applicability of the fully-rough velocity profile in the overlap region; the following derivation also considers the outer region by accounting for the favorable pressure gradient

$$U^+(z) = \frac{1}{\kappa} \ln \left( \frac{z}{\eta_{rms}(x)} \right) + 8.5 + \frac{2\Pi}{\kappa} \sin^2 \left( \frac{\pi z}{2\delta} \right) \quad (7)$$

where  $\Pi$  is Coles' parameter. Equation (6) can be expressed as:

$$\frac{d\delta}{dx} = \frac{F - \delta \frac{\partial G}{\partial \Pi} \frac{d\Pi}{dx}}{G} \quad (8)$$

where  $G = \frac{\Pi^2 - 4 - 4\Pi(1+\Pi) - 4\Pi Q/\pi}{2(\kappa U_0^+)^2} + \frac{1+\Pi}{\kappa U_0^+}$ ,  $F = \frac{1}{U_0^+} \left( 1 - \frac{2\delta_2 + \delta_1}{\delta} \right)$  and  $Q = \int_0^\pi \sin(z)/z dz = 1.85$ . This equation can be integrated numerically for a given  $U_0^+ = \sqrt{2/c_f}$  and  $\Pi$ . The result of the equation is an expression for the boundary layer thickness  $\delta = \Phi(x, c_f, \Pi)$ . Based on equation (7) at  $z = \delta$ , we obtain a relation between the surface elevation and the skin friction:

$$\eta_{rms} = \frac{\Phi(x, c_f, \Pi)}{e^{\kappa(U_0^+ - 8.5 - 2\Pi(x)/\kappa)}} \quad (9)$$

The reader is referred to Geva & Shemer (2022) for detailed derivation.

For all cases listed in Table 1, equation (8) was solved numerically by a 4<sup>th</sup> order Runge-Kutta routine with the experimentally obtained dependence  $\Pi(x)$  and the initial value of  $\delta \approx 0.05$  m at  $x = 1$  m. Estimates of spatial evolution of  $\eta_{rms}$  for a given wind forcing were found using equation (9)

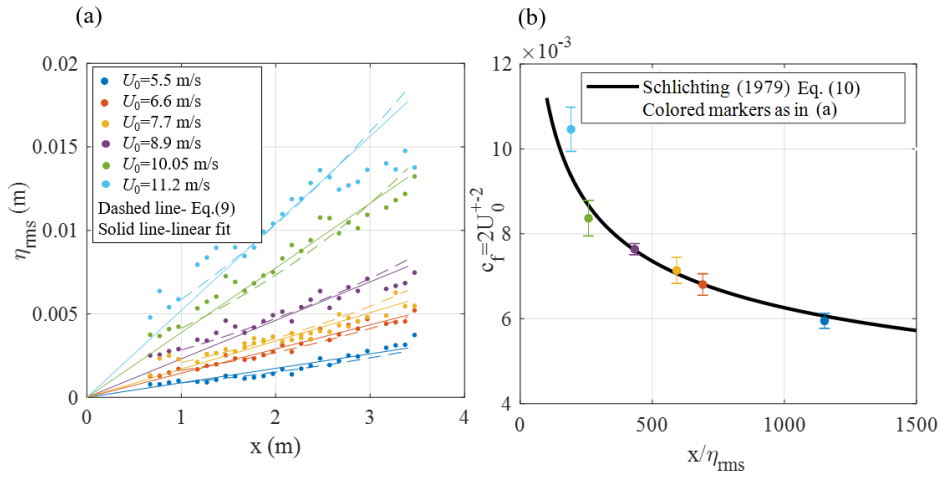


Figure 7. The coupling between air flow and the growth of young wind waves: (a) surface elevation as a function of  $x$  for various wind velocities and (b) Skin-friction coefficient dependence on  $x/\eta_{rms}$ .

and plotted in figure 7(a) with broken lines. The results compare reasonably well with measurements of the surface elevation for various wind velocities (dot markers). Linear fits were added as well, demonstrating that at each wind velocity  $U_0$ , the characteristic amplitude of the surface elevation grows nearly linearly with  $x$ , so that  $x/\eta_{rms}$  remains approximately constant. This supports the observation of constant with  $x$  skin-friction for a given wind velocity reported by previous studies; it is similar to the case of the developing boundary layer over solid surface where the effective roughness grows linearly with  $x$  (Sridhar *et al.*, 2017). Estimates of  $x/\eta_{rms}$  based on the slopes of the linear fits (Figure 7a) for a given  $c_f$  are displayed by colored markers in Figure 7(b). This figure compares results with skin friction estimation based on:

$$c_f = [2.87 + 1.58 \log_{10}(x/k_s)]^{-2.5} \quad (10)$$

that was obtained over solid rough surface with constant  $k_s$  and without pressure gradient (Schlichting, 1979). Surprisingly, reasonable agreement was found. It should be mentioned that we do not present the skin friction values as a function of  $Re_x$  as is common for flows over rough solid surface. Instead, in wind waves studies, the nondimensional fetch,  $xg/u_*^2$  is customarily used. The dependence of the drag coefficients on the nondimensional fetch is presented in Geva & Shemer (2022) and compared with numerous results available elsewhere. The values of the drag coefficients in our experiments agree well with those data.

## CONCLUSIONS

In wind-waves studies, the coupling between air flow and the developing wave field is crucial in estimation of mass, momentum and energy transfer between both phases. So far, the majority of wind-waves studies had focused mainly on the water parameters. This study was dedicated to the analysis of the developing boundary layers over wind waves in relations to the local wave conditions. We have examined 42 different cases covering 6 wind forcings and 7 spatial locations. It was demonstrated that the boundary layers over wind waves maintain wall similarity; the local characteristic surface elevation serves as the equivalent sand grain roughness. The momentum

integral equation was used to provide an independent robust evaluation of friction velocities. These values were found to agree well with estimates in previous study that used different techniques. The friction velocities determined by the integral method remain nearly constant along the test section even though the boundary layer develops with  $x$ . More importantly, we use the momentum integral equation to express the drag coefficients that characterize the coupling between airflow and water surface. The experiments show that for a given wind forcing, the rms value of the surface elevation grows nearly linearly with downstream distance. This linear growth of the characteristic wave amplitude is consistent with the case of linear increase in solid roughness height which results in constant skin-friction coefficients. The skin friction coefficients in this study were found to agree well with the relation of skin friction dependence with  $x/k_s$  over rough solid surface. This study provides an alternative approach to study the coupling between wind and waves and offers a new understanding of the relation between the drag coefficients and the local surface conditions.

## Acknowledgement

This study was supported by grant # 508/19 from Israel Science Foundation.

## REFERENCES

- Buckley, M. P., Veron, F. & Yousefi, K. 2020 Surface viscous stress over wind-driven waves with intermittent airflow separation. *J. Fluid Mech.* **905**, A31.
- Bye, J. A. T., Ghantous, M. & Wolff, J. O. 2010 On the variability of the charnock constant and the functional dependence of the drag coefficient on wind speed. *Ocean Dyn.* **60** (4), 851–860.
- Castro, I. P. 2007 Rough-wall boundary layers: Mean flow universality. *J. Fluid Mech.* **585**, 469–485.
- Caulliez, G., Makin, V. & Kudryavtsev, V. 2008 Drag of the water surface at very short fetches: Observations and modeling. *J. Phys. Oceanogr.* **38** (9), 2038–2055.
- Charnock, H. 1955 Wind stress on water surface. *Q. J. R. Meteorol. Soc.* **81**, 639–640.
- Chung, D., Hutchins, N., Schultz, M. P. & Flack, K. A. 2021 Predicting the drag of rough surfaces. *Annu. Rev. Fluid Mech.* **53**, 439–471.

- Csanady, G. T. 2001 *Air-Sea Interaction*. Cambridge: Cambridge University Press.
- Flack, K.A. & Schultz, M. P. 2014 Roughness effects on wall-bounded turbulent flows. *Phys. Fl.* **104**, 101305.
- Geva, M & Shemer, L. 2022 Wall similarity in turbulent boundary layers over wind waves. *J. Fluid Mech.* **935**, A42.
- Hristov, T. S., Miller, S.D. & Friehe, C. A. 2003 Dynamical coupling of wind and ocean waves through wave-induced air flow. *Nature* **422** (6927), 55–58.
- Hsu, C.T, Wu, H. Y., Hsu, E. Y. & Street, R. L. 1982 Momentum and energy transfer in wind generation of waves. *J. Phys. Oceanogr.* **12** (9), 929–951.
- Jimenez, J. 2004 Turbulent flows over rough walls. *Annu. Rev. Fluid Mech.* **36**, 1731–196.
- Kumar, K., Singh, S. K. & Shemer, L. 2022 Directional characteristics of spatially evolving young waves under steady wind. *Phys. Rev. Fluids* **7**, 014801.
- Liberzon, D. & Shemer, L. 2011 Experimental study of the initial stages of wind waves' spatial evolution. *J. Fluid Mech.* **681**, 462–498.
- Miles, J. W. 1957 On the generation of surface waves by shear flows. *J. Aero. Sci.* **24**, 704.
- Plant, W.J. & Wright, J. W. 1977 Growth and equilibrium of short gravity waves in a wind-wave tank. *J. Fluid Mech.* **82** (4), 767–793.
- Schlichting, H. 1979 *Boundary-Layer Theory*. Cambridge: McGraw-Hill.
- Schultz, M. P. & Flack, K. 2007 The rough-wall turbulent boundary layer from the hydraulically smooth to the fully rough regime. *J. Fluid Mech.* **580**, 381–405.
- Shockling, M. A., Allen, J. J. & Smits, A. J. 2006 Roughness effects in turbulent pipe flow. *J. Fluids Mech.* **564**, 267–285.
- Sridhar, A., Pullin, D.I. & Cheng, W. 2017 Rough-wall turbulent boundary layers with constant skin friction. *J. Fluid Mech.* **818**, 26–45.
- Zavadsky, A. & Shemer, L. 2012 Characterization of turbulent airflow over evolving water-waves in a wind-wave tank. *J. Geophys. Res.* **117**, C00J19.
- Zavadsky, A. & Shemer, L. 2017 Investigation of statistical parameters of the evolving wind wave field using a laser slope gauge. *Phys. Fluids* **29**, 056602.